Earthquake Spectra

RESEARCH PAPER

Vertical-Component Seismic Response and System Identification of a 52-Story High-Rise Building Using Earthquake Data

Viviana Vela[1] | Farid Ghahari[1] | Monica D. Kohler[2] | German A. Prieto[3] | Ertugrul Taciroglu[1]

[1]University of California, Los Angeles, California, USA | [2]California Institute of Technology, Pasadena, California, USA | [3]Universidad Nacional de Colombia, Bogotá, Colombia

Correspondence: Viviana Vela (vivianavela@ucla.edu)

Received: 12 June 2025 | **Revised:** 3 November 2025 | **Accepted:** 15 December 2025

Keywords: beating phenomenon | instrumented structures | structural monitoring | system identification | tall building | vertical modes of vibration | vertical seismic response

ABSTRACT

This study investigates the vertical dynamic response of a 52-story high-rise building in downtown Los Angeles using small-magnitude earthquake data recorded by the Community Seismic Network. While seismic design traditionally emphasizes horizontal ground motion, vertical accelerations can have a significant impact on tall structures, leading to amplification effects and complex wave propagation. Using data-driven techniques, such as subspace system identification, spectral analysis, and transfer function (TF) estimation, we identify a global vertical mode at approximately 1.86 Hz, along with a potential secondary mode and beating phenomena. Results indicate that vertical-component motions can influence structural response and design considerations, particularly in buildings with dual lateral systems. Our findings contribute to a deeper understanding of vertical seismic effects on high-rise buildings, emphasizing the need for a more sophisticated treatment of these effects in earthquake engineering.

1 | Introduction

Earthquake design and analysis have primarily focused on lateral dynamic response; however, studies have shown that vertical structural dynamics play a larger role in force redistribution and building performance than previously assumed, presuming a building has adequate vertical stiffness. Observations from recent earthquake recordings, such as from the 2016–2017 central Italy and 2023 Turkey-Syria earthquake sequences, have shown that the vertical component of ground motion, which is typically assumed to be lower (about two-thirds) in amplitude than the horizontal component, can actually be larger for both near-fault and far-fault locations (Marotti et al. 2024; AFAD 2023). There are many highly developed metropolitan centers and cities with high-rise buildings in earthquake-prone areas. Here, we present a comprehensive investigation of the currently understudied vertical responses of systems involving both lateral and axial elements, utilizing seismic recordings from a well-instrumented high-rise building.

Past research has highlighted the relevance of vertical seismic effects; however, as this developing field continues to grow, more focused attention has led to recent findings that provide additional insight into the dynamic factors influencing vertical elements and the extent of their impact. Observations from field measurements have confirmed vertical acceleration amplification effects along the height of structures due to vertical-component ground shaking (Bozorgnia et al.

1998; Furukawa et al. 2013; Ryan et al. 2016). These studies have indicated continuous acceleration amplification along the height of the building, with the highest amplifications seen at or around the roof level. Numerical studies that have incorporated both horizontal and vertical ground motions in earthquake analysis have confirmed that this combination results in increased structural demands for vertical elements (Boroschek and Cares 2020; Chen and Moehle 2024). This typically results in additional structural reinforcement needed to accommodate the increased axial demands. Research efforts have also focused on peak vertical acceleration demands for various lateral system layouts and compared their values at different locations along structural elements (Moschen et al. 2016; Gremer et al. 2019; Acosta et al. 2023, 2024). The increased peak vertical acceleration demands in a floor system can vary spatially, making it critical to understand these effects on acceleration-sensitive elements such as nonstructural components. Although numerical studies provide valuable insight into possible dynamic vertical behavior, the results will depend on how certain properties are modeled. For example, damping type and value, along with mass distribution, are components that significantly affect analysis results and can lead to underestimation of vertical building response if not considered accurately (Boroschek and Cares 2020; Gremer et al. 2023).

In a typical code-based design, vertical earthquake consideration is overly simplistic: it is treated as an additional static load. In ASCE 7, it is defined as 20% of the product of the short-period design spectral acceleration S_{DS} and the design dead load (ASCE 7–22). The code now incorporates the option to use a vertical elastic design response spectrum. However, this is not often used in practice, as there is limited guidance on incorporating it into modeling and analysis, and it is typically assumed that the building is already sufficiently stiff in the vertical direction. While prior studies have analyzed vertical structural dynamics numerically or analytically, validation studies using real-world data are necessary for obtaining reliable results. Seismic response measurements from instrumented buildings can provide the necessary basis for refining current code provisions, offering clearer guidance on incorporating vertical seismic effects into design practices.

Vertical modes of vibration along the height of a building can be highly sensitive to the local vibration modes of the structure, such as those associated with the slab and floor system. One objective of this study is to identify the global vertical structural modal properties of the targeted 52-story instrumented building. Among the few studies on identifying vertical modes, Aihemaiti et al. (2023) examined transfer functions (TF) derived from microtremor data from a densely instrumented, 50-story, full-scale testbed site in Kunming, China, to identify horizontal, torsional, and vertical structural modes. Their analysis revealed complex and closely spaced vertical modes. When modeling an inelastic 20-story steel moment-frame building, Hall (2018) identified several vertical and *vertically adjacent* modes of vibration, with a cluster of 12 modes occurring at periods of 0.18 s or less. Such observations further indicate that vertical ground motion excites structural components, and the presence of multiple, closely spaced vertical modes complicates the response, making accurate damping and response predictions more challenging (Acosta et al. 2024).

With increasing sensor availability, state-space model representations for system identification that rely on time-series data have been adapted for structural engineering applications to estimate modal characteristics (i.e., natural frequencies, damping ratios, and mode shapes) (Smyth et al. 2003; Skolnik et al. 2005; Thai et al. 2007; Ghahari et al. 2013; Reinoso and Miranda 2005; Sun et al. 2023). These modal data can subsequently be used for model updating and have been utilized in structural health monitoring to identify damage (Loh and Loh 2019; Döhler et al. 2014). Using vertical motion observations from our specimen building, this study employs subspace state-space system identification with several small-magnitude earthquakes to characterize the fundamental global vertical axial mode and to estimate a possible second vertical mode.

The beating phenomenon, which arises when two closely spaced vibration frequencies interact, can contribute to fatigue in structural elements by increasing the duration and amplitude of the vibration. With a vertical wave propagating through structural elements such as columns, axial loading will fluctuate as the demands on the members increase and decrease. Increased and cycled axial demands will cause strain and fatigue on connections. In steel structures, long-term strength degradation in connections could occur. Decreasing axial loads will reduce confinement in reinforced concrete members and may cause momentary reductions in lateral capacity. Studies have investigated structural beating (Boroschek and Mahin 1991; Çelebi 2004, 2006, 2007; Çelebi et al. 2016); however, to the best of the authors' knowledge, prior studies have not addressed beating in the vertical direction, nor have they provided theories on its probable causes. We present spectrograms of the vertical acceleration signals, which provide a more complete picture for determining when the beating of closely spaced vertical modes is (or is not) occurring during seismic excitation. We explore possible mechanisms underlying this beating effect, particularly in relation to the dual lateral system and other dynamic characteristics that may be causing the modal coupling. We also examine how the excited vertical frequencies vary over time in smaller-magnitude earthquakes and explore their potential implications for long-term structural performance. The existing literature on temporal variations in modal properties has primarily focused on lateral dynamic properties (Todorovska and Trifunac 2008; Prieto et al. 2010; Rahmani et al. 2015; Peng and Ben-Zion 2006; Nakata and

Snieder 2014; Prieto and Kohler 2024); here, we extend this to vertical dynamics. Using time-domain, frequency-domain, and system representation methods applied to high-resolution and spatially dense sensor data, we can extract vertical modal characteristics, detect time-varying mode frequency shifts, and capture beating.

The type of earthquake-resisting lateral system of the specimen building in this study is common in many tall buildings in seismically active urban regions along the U.S. West Coast, particularly in the Los Angeles area. It is, therefore, representative of what can be expected more generally for the vertical dynamic behavior of buildings with this lateral system. The results presented here, from several data-driven approaches using spatially dense acceleration sensor data from an instrumented 52-story structure, add to the otherwise sparse real-world data analyses of vertical structural dynamics and enhance our understanding of phenomena that should be considered when examining vertical seismic effects. Simple empirical factors alone will not accurately predict vertical response, and the evidence of vertical beating and temporal modal variations presented here suggests the need for dynamic analysis in three dimensions to understand the impacts on resonance and fatigue for different types of building structures. With further insight into the mechanisms that may contribute to such phenomena and how building type properties such as height, lateral system, and materials contribute, we can better inform how to incorporate them for improved design.

2 | Instrumented Building and Data Description

The instrumented 52-story office building that is the focus of this study was constructed in the late 1980s. Like many mid- and high-rise buildings in downtown Los Angeles, it is constructed with a dual lateral force-resisting system. Combining two lateral systems creates a more advantageous (albeit complex) distribution of member forces in seismic design. The building is one of the few high-rise buildings exceeding 200 m, with an average story height of about 4 m. The structural framing of the 52-story building consists of a central core of steel-braced frames and moment frame beams. A typical floor plan, shown in Figure 1, displays the orientation of the seismic framing system. Above ground, the building is symmetric about its principal building-East-West (EW) and building-North-South (NS) axes. The moment frame connections in both directions are welded, unreinforced flange connections. Typical element types include wide-flange steel beams and braced frames, while columns consist of a combination of wide-flange or built-up sections. Structural steel framing utilizes ASTM A572 Grade 50 for most rolled shapes, with ASTM A36 specified for steel plates. Typical moment-connected beams in the building are W36 sections. The floor and roof diaphragms consist of a metal deck with concrete fill. These framing characteristics are generally consistent throughout the height of the building. Additional details are available in the studies by Kohler et al. (2016) and Taranath (1997).

This office building in downtown Los Angeles features 60 triaxial sensors (180 channels), distributed approximately one per floor, spanning the lowest subterranean garage level to the roof level, with additional sensors at selected floors for redundancy. Sensors are mounted near the central core, between the northeast and southeast corner column lines of the building (Figure 1).

Each sensor node is part of the Community Seismic Network (CSN), whose sensors have been deployed in over 1,300 ground-level and upper-floor locations in low-, mid-, and high-rise buildings (Clayton et al. 2011; Clayton et al. 2015; Clayton et al. 2020; Prieto and Kohler 2024; Kohler et al. 2014, 2020). The CSN sensor array consists of triaxial MEMS accelerometers with a ±2 g range, 16-bit resolution, and sensitivity of 70 $\mu g/\sqrt{Hz}$, integrated with a Raspberry Pi microcomputer for on-site processing and cloud communication. The raw acceleration signal is sampled at 250 Hz and then downsampled to 50 Hz prior to storage and transmission to a cloud storage service. This enables continuous recording of both strong-motion earthquakes and low-amplitude ambient and small-magnitude vibrations in near real time. The data acquisition operates in a continuous mode that uploads 10-minute waveform segments to an Amazon Web Services cloud archive and then to an archive at Caltech. All stations are time-synchronized using Network Time Protocol, achieving timing accuracy of 0.02 s or better, which is essential for multi-floor installations. Each sensor package is equipped with a small uninterruptible power supply that provides several hours of backup operation in the event of a power outage (Kohler 2021).

As a result of the continuous acceleration recordings by CSN sensors, many low-amplitude earthquakes have been captured and are used in this study. In addition, ambient vibration data are introduced and utilized to characterize the building's response under stationary excitation. These ambient segments provide a reference estimate for the fundamental modal frequencies under elastic conditions, complementing the earthquake-based system identification. Earthquake data recorded by CSN are used here that met the criteria of having: i) a moment magnitude (Mw) greater than 4, ii) epicentral distance less than 70 km, and iii) peak vertical-to-horizontal (V/H) acceleration greater than 0.5. The peak V/H ratio is calculated using data from the lowest above-grade instrumented level, Floor 2 (F2), which provides the closest

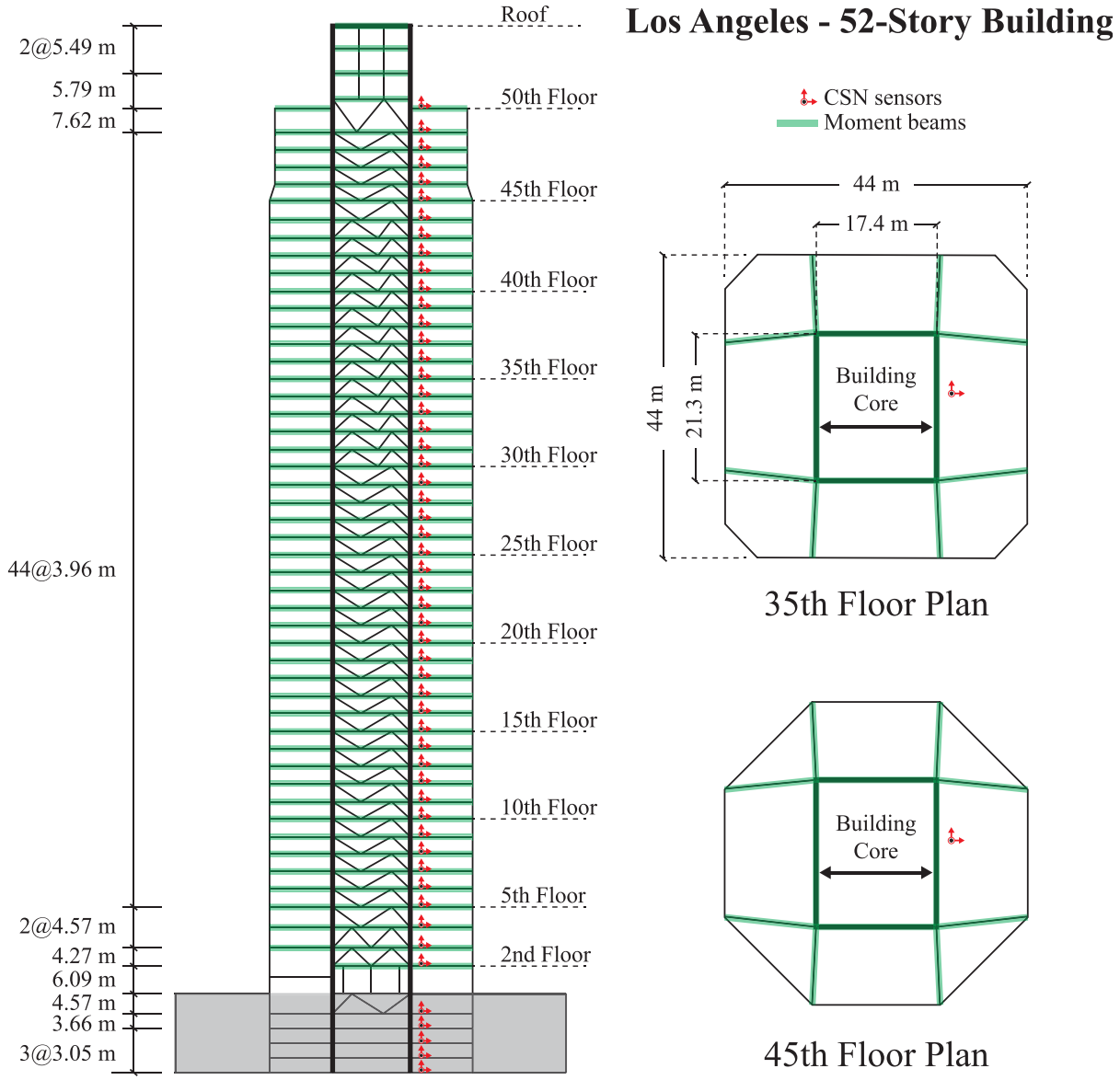

FIGURE 1 | Elevation view of the building's EW frame system and typical floor plan schematic of the 52-story high rise. EW = East–West.

available floor reflecting input motion representative of the building base excitation. For each event, the peak V/H ratio is computed as the peak vertical acceleration divided by the larger of the two horizontal components recorded at F2. Although the 0.5 criterion is not a strict threshold, it serves as a practical indicator of events exhibiting relatively strong vertical energy compared with their horizontal counterparts. Table 1 shows relevant details for the selected earthquakes used in this study. Figure 2 shows the locations of these earthquakes relative to the location of the 52-story high-rise.

The building is located within the central Los Angeles Basin, a broad structural depression filled with sedimentary layers that deepen toward its center. The thick sedimentary deposits have been known to amplify long-period ground motions. According to the USGS time-averaged shear-wave velocity in the upper 30 m (V_{S30}) database, the local site corresponds approximately to Site Class D, per ASCE 7, based on a V_{S30} of about 350 m/s derived from regional mapping (USGS 2020).

Acceleration data used here are detrended and bandpass-filtered using a 3-pole Butterworth filter with zero phase distortion and cut-off frequencies of 0.1 and 10 Hz to eliminate non-seismic noise. Figures 3 and 4 show the vertical acceleration recordings and their Fourier amplitude spectra as a function of building height for the 2023 Malibu and 2024 Highland Park earthquakes; figures for the other events in Table 1 are in the Supporting Information (Figures S1 and S7). Since there is no sensor at the true ground level, we evaluated both the first above-grade instrumented floor level Floor 2 (F2) and the first subterranean level 1 (B1) as proxies for ground level for system identification and TF estimation.

TABLE 1 | Earthquakes used in this study.

Event location	Date	Mw	Distance from building, km	NS PGA, %g	EW PGA, %g	Vertical PGA, %g
Pacoima, CA	07/30/2020	4.2	32	0.49	0.50	0.38
Malibu, CA	01/25/2023	4.2	45	0.23	0.25	0.23
Malibu, CA	02/09/2024	4.6	60	0.33	0.36	0.27
Highland Park, CA	08/12/2024	4.4	8	3.78	2.20	1.16

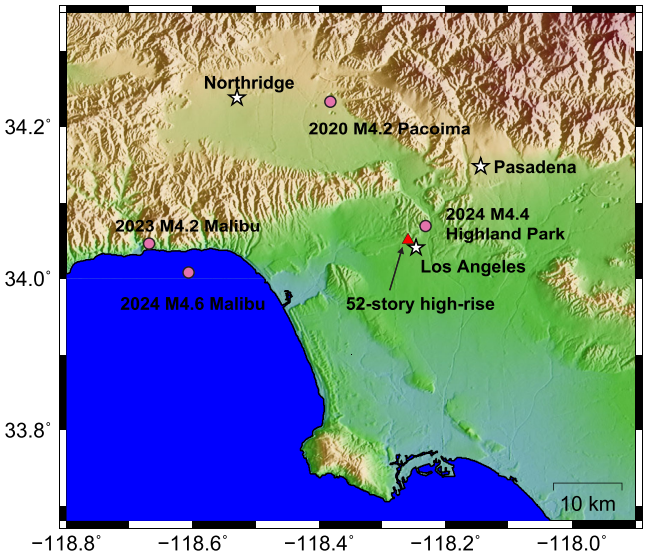

FIGURE 2 | 52-story high-rise location (red triangle) and four selected earthquake locations (pink circles). City locations are indicated by white stars next to city names.

Comparisons showed that the frequency content and amplitude ratios obtained using F2 and B1 as references are very similar for the primary modes of interest. We therefore adopted F2 as the reference level in the analyses presented herein to focus on the above-grade structural response and avoid any potential basement–level interaction effects.

3 | Vertical System Identification and Modal Analysis

3.1 | Methodology

Subspace system identification, also referred to as "system identification" throughout this paper, is a data-driven approach that utilizes subspace methods to determine the state-space parameters of a dynamic system. It estimates the state vectors by making projections of certain subspaces generated from input–output data and solving the least-squares problem for state-space realizations. Input and output data are typically in the form of time-series measurements. The transformation of the second-order differential equation of motion that governs the dynamic behavior of a structural system into a first-order state-space form allows for the direct connection to experimental data, achieved with a state vector $z(t)$:

$$z(t) = \begin{bmatrix} x(t) \\ \dot{x}(t) \end{bmatrix} \tag{1}$$

where in classical structural dynamics $x(t)$ = displacement and $\dot{x}(t)$ = velocity. Due to the discrete-time nature of data collection, a conversion from continuous-time, state-space representation to a discrete-time model is necessary. The discrete-time, state-space equations can be written as

$$z[n+1] = \boldsymbol{A}_d z[n] + \boldsymbol{B}_d f[n] \tag{2}$$

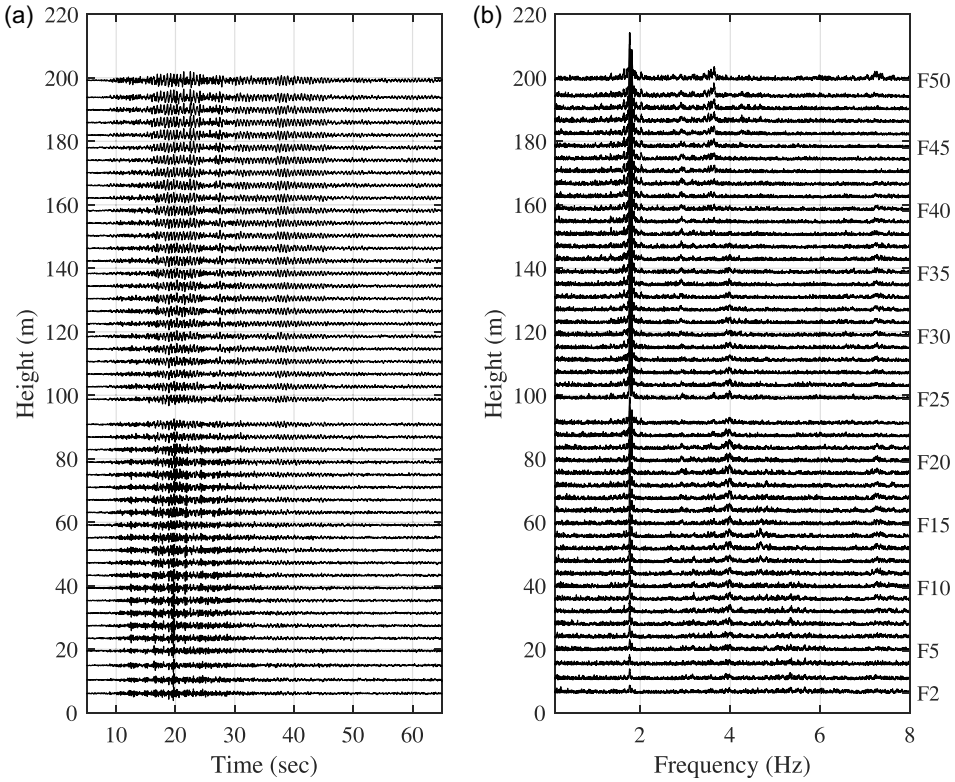

FIGURE 3 | (a) Acceleration time histories and (b) Fourier amplitude spectra from Floors 2 and above from the vertical component of the CSN sensors in the 52-story building in downtown Los Angeles during the 2023 M4.2 Malibu earthquake. Acceleration amplitudes are scaled by the same constant to show comparable relative amplitudes as a function of height. CSN = Community Seismic Network.

$$y[n] = \boldsymbol{C}z[n] + \boldsymbol{D}f[n] \tag{3}$$

where $\boldsymbol{A}_d$ = discrete-time system matrix, $\boldsymbol{B}_d$ = discrete-time input matrix, $\boldsymbol{C}$ = output matrix, and $\boldsymbol{D}$ = feedthrough matrix. Since our study deals with absolute accelerations, the feedthrough matrix ($\boldsymbol{D}$) is set to zero. Subspace system identification techniques can reconstruct internal states from acceleration input–output data and estimate the state-space matrices directly from the measured signals without requiring prior knowledge of system parameters. Once the discrete-time system matrices are identified, they must be converted back to their continuous-time ($\boldsymbol{A}_c, \boldsymbol{B}_c, \boldsymbol{C}, \boldsymbol{D}$) counterparts. Under the assumption of small and classical damping, and given that the building remains in the linear elastic range under small-magnitude ground motions, the relevant modal properties such as natural frequencies f_n, mode shapes Φ_n, and damping ratios ζ_n can be approximated:

$$f_n = \frac{|\lambda_n|}{2\pi} \tag{4}$$

$$\Phi_n = |\boldsymbol{C}\phi_n| \cdot \mathrm{sign}(\mathrm{Re}(\boldsymbol{C}\phi_n)) \tag{5}$$

$$\zeta_n = \frac{|\mathrm{Re}(\lambda_n)|}{\sqrt{\mathrm{Re}(\lambda_n)^2 + \mathrm{Im}(\lambda_n)^2}} \approx \frac{|\mathrm{Re}(\lambda_n)|}{2\pi f_n} \tag{6}$$

where λ_n, ϕ_n are the complex eigenvalues and eigenvectors of the system matrix $\boldsymbol{A}_c$, respectively (Ljung 1999; Juang 1994; Alvin and Park 1994).

We use the subspace state-space system identification (N4SID) algorithm (Van Overschee and De Moor 1994) due to its numerical robustness for modeling the vertical dynamic properties of the 52-story building. For our purposes, state-space models are considered linear, time-invariant and discrete time, which is a reasonable assumption since the building response is expected to remain predominantly in the elastic range for small-magnitude events. The primary objective of the system identification is to estimate the global frequency range associated with the dominant vertical motion and

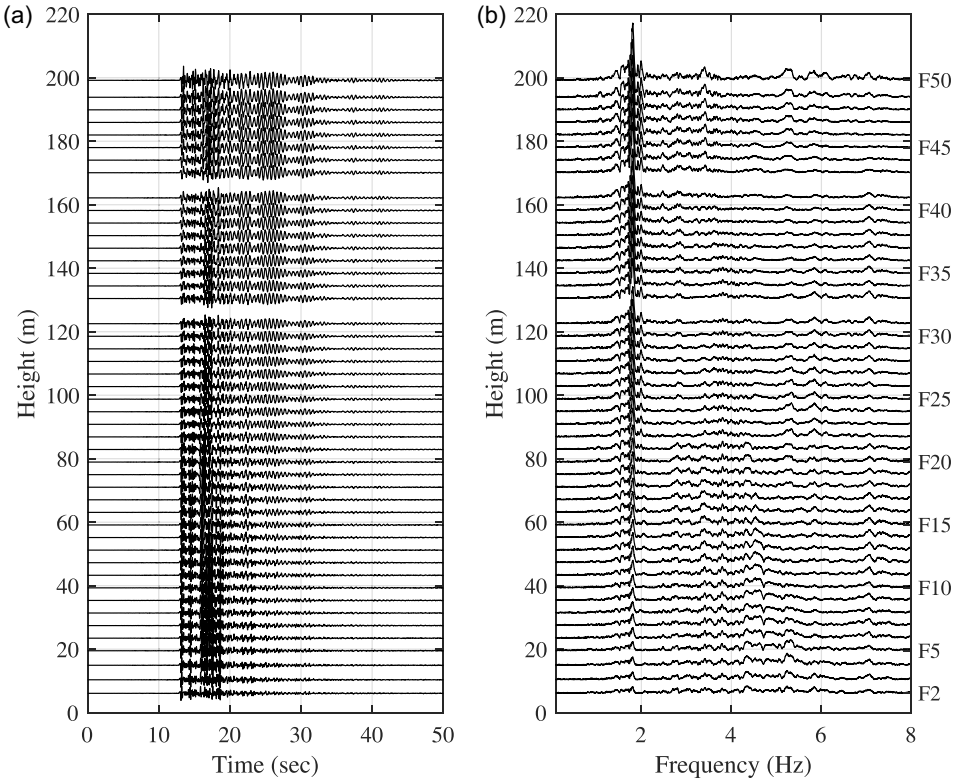

FIGURE 4 | (a) Acceleration time histories and (b) Fourier amplitude spectra from Floors 2 and above from the vertical component of the CSN sensors in the 52-story building in downtown Los Angeles during the 2024 M4.4 Highland Park earthquake. Acceleration amplitudes are scaled by the same constant to show comparable relative amplitudes as a function of height. CSN = Community Seismic Network.

characterize the average behavior of this mode over the selected analysis time windows. For stronger ground motions that could induce nonlinear or stiffness-degradation effects, other time-varying system identification approaches could be employed to capture evolving modal characteristics; however, such methods are not presented in this study. A single-input, multiple-output system modal identification is used here to focus solely on the dynamics governed by vertical accelerations. The vertical system is assumed to be a deterministic model. Only vertical acceleration recordings are considered for the system, with input signal from Floor 2 (F2) and the output signals from the floors above (F3, F4,...). Subterranean level measurements are not used since the focus is on structural behavior above ground level.

To implement the N4SID algorithm, the order of the states to be considered must be determined; this can be a challenging problem as the number of degrees of freedom and free parameters increases. We consider the vertical response recorded at 48 floors (F3-F50), assuming we have all floor recordings during the event, resulting in 48 measured output channels. Since the building's number of true physical vertical degrees of freedom exceeds the number of sensors, the identified model is a reduced-order representation. We carry out N4SID analyses for model orders up to 160, and the final order is selected from stability diagrams and comparisons with validation sets.

Stability criteria are chosen to focus on changes in estimated frequencies, damping ratios, and modal assurance criterion (MAC) and to distinguish stable modes from modes that are not consistent with increasing model order. Stability plots are created using tolerances: $\Delta f < 2\%$, $\Delta \zeta < 20\%$, and $\mathrm{MAC} > 99\%$.

3.2 | System Identification Results

The results presented here focus on data from two earthquakes: the 2023 M4.2 Malibu and the 2024 M4.4 Highland Park, which are presented as representative examples (see Table 1). Similar results and figures are shown in the Supporting Information for the 2020 M4.2 Pacoima (Figure S2) and 2024 M4.6 Malibu (Figure S7) earthquakes. Each earthquake is analyzed independently to update a model using the system identification algorithm, and accuracy is validated with the remaining events. Separate input–output datasets are used for each event since the available floor signals differ slightly when a CSN sensor or two is down during each earthquake. This approach allowed for the direct assessment of the reproducibility of the dominant vertical mode across multiple events, despite small variations in the measured degrees

of freedom. Figures 5 and 6 display the stability plots for modal identification using data from the 2023 Malibu and 2024 Highland Park earthquakes, respectively. The 2023 Malibu event clearly captures a stable frequency at around 1.83 Hz, which is investigated as a potential global vertical mode. The stable frequency around 3.6 Hz is the next frequency of interest. It is investigated as a potential second vertical mode, as it also appears in the system identification results for other events (see Supporting Information, Figures S2 and S8). For the Highland Park event, the stability plot shows two dominant modes between 1.5 and 2 Hz. The dominant frequency near 1.5 Hz is not seen in the Fourier amplitude spectra or the TF reported in later sections, suggesting that it does not represent a dominant global vertical mode. Instead, its isolated appearance in the system identification results may reflect a weakly participating torsional or mixed torsional-vertical response, since system identification focuses on correlated input–output data rather than just amplitude peaks. Since this feature is not repeated in other events, it is interpreted as a secondary system response rather than a recurring global vertical mode response.

3.3 | Mode Validation and Cross-Comparison

In addition to stability plots, one way to assess the accuracy of estimated state-space model parameters is to verify their predictions against other available data. Each seismic event is analyzed independently to train its own system, which is then validated using the remaining earthquake data. It is necessary to construct separate systems with the input–output datasets, given the inherent variability in the systems due to minor variations in the available floor recordings. The two systems identified using the 2023 M4.2 Malibu and 2024 M4.4 Highland Park datasets, respectively, are tested for their responses to the remaining earthquakes listed in Table 1. The results for systems generated from the other earthquakes can be found in the Supporting Information (Figures S3 and S9).

A model order of 68 is selected based on trends with small root–mean-square errors and standard deviations when comparing Fourier amplitudes of the earthquake data and model results. Despite the differences in degrees of freedom across individual event datasets, the identified vertical modes show robustness across similar model orders. The model order selected yields approximately 50% goodness-of-fit for the dominant vertical mode frequency when validated against the

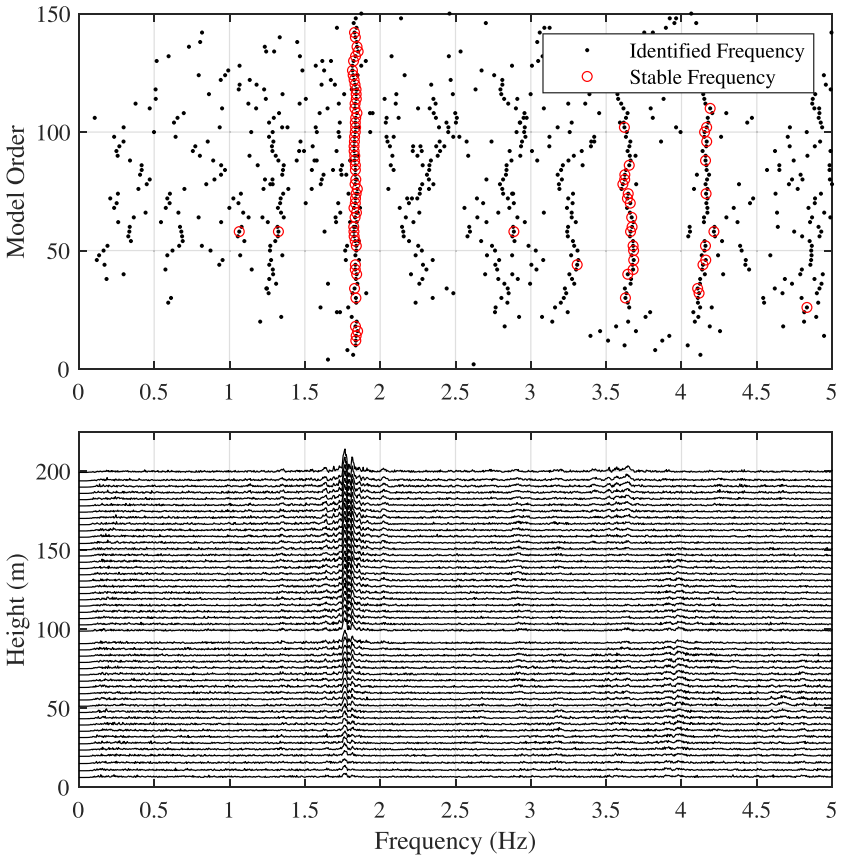

FIGURE 5 | Stability plot (top) for system identification results from recorded responses to the 2023 M4.2 Malibu earthquake and Fourier amplitude spectra (bottom). The stability criteria are $\Delta f < 2\%$, $\Delta \zeta < 20\%$, MAC $> 99\%$.

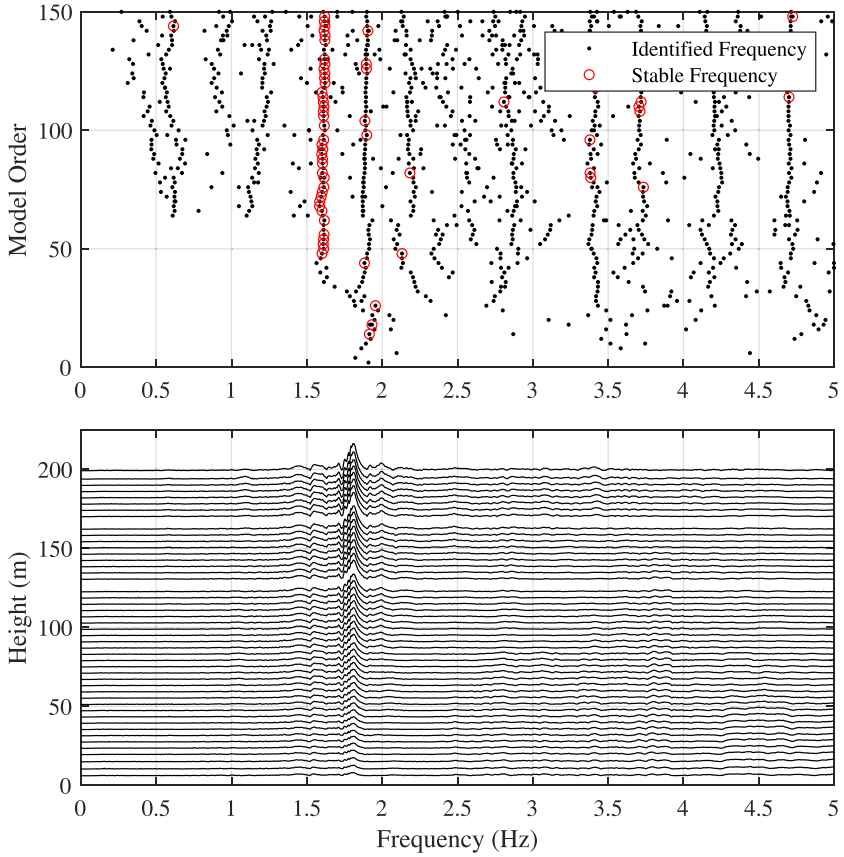

FIGURE 6 | Stability plot (top) for system identification results from recorded responses to the 2024 M4.4 Highland Park earthquake and Fourier amplitude spectra (bottom). The stability criteria are $\Delta f < 2\%$, $\Delta \zeta < 20\%$, MAC $> 99\%$.

remaining independent datasets, which is reasonable given the low amplitude of the recordings. Although a lower model order may be justified for certain events, a consistent model order is adopted to maintain comparability across systems, given that only one or two floor signals are missing between datasets. This helps to ensure that any variations in modal parameters primarily reflect structural behavior rather than differences in model order. Figure 7 illustrates the system response in both the time and frequency domains at Floor 36, compared to the direct earthquake data. Floor 36 is chosen as an example mid-to-upper height level in the structure where vertical-mode amplitudes become evident. Similar agreement between predicted and recorded responses is observed on other instrumented floors. Stable modes associated with model order 68 are extracted, and Table 2 summarizes the global fundamental frequency for predominantly vertical motion detected by the system identification mode shape results. The combined results indicate that a stable frequency is detected around 1.86 ± 0.03 Hz.

Each system identification model yields a slightly different fundamental vertical frequency because observed frequencies vary from earthquake to earthquake. In addition, the models each reflect slightly different subsets of observations (e.g., missing floors due to nonfunctioning sensors at the time of the earthquake). However, the stable mode detected corresponds to an overall global vertical mode shape with consistently increasing amplitudes with height, representing the relative vertical displacement amplitude at each instrumented level (Figure 8). The mode shape illustrates the distribution of vertical motion along the height, rather than the in-plane deformation of the building, since there is only one sensor on each floor level. We attribute this to a global mode and not a floor slab mode because local slab modes would likely show either inconsistent directionality on a floor-to-floor basis or approximately the same deflection at all floors.

The damping ratios reported in Table 2 show relatively low values (ranging from $\sim$1% to 3.5%) suggesting minimal energy dissipation in the vertical direction, which may increase the potential for resonance during repeated excitation. These values should be interpreted with an understanding of their inherent uncertainty. Based on our stability criterion ($\Delta \zeta < 20\%$), these estimates are considered reliable, although damping can be more sensitive to noise and model order than frequency. The ability to obtain empirical vertical damping estimates from real building data represents a significant advantage of this approach, particularly given the limited availability of vertical damping values in full-scale structures.

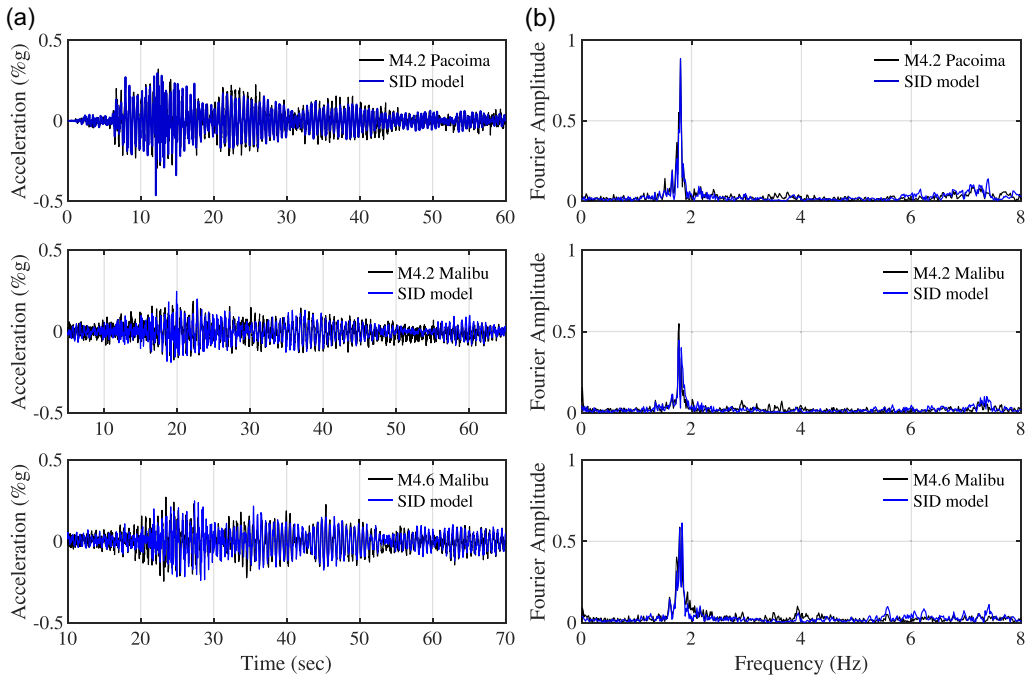

FIGURE 7 | Comparison of N4SID model results with data for Floor 36 from the earthquakes. (a) Acceleration time series and (b) Fourier amplitude spectra.

TABLE 2 | Detected stable vertical frequency from system identification analysis associated with vertical motion.

Event	Fundamental frequency, Hz	Damping, %
2020 M4.2 Pacoima	1.86	2.3
2023 M4.2 Malibu	1.83	3.5
2024 M4.6 Malibu	1.86	1.1
2024 M4.4 Highland Park	1.88	1.7

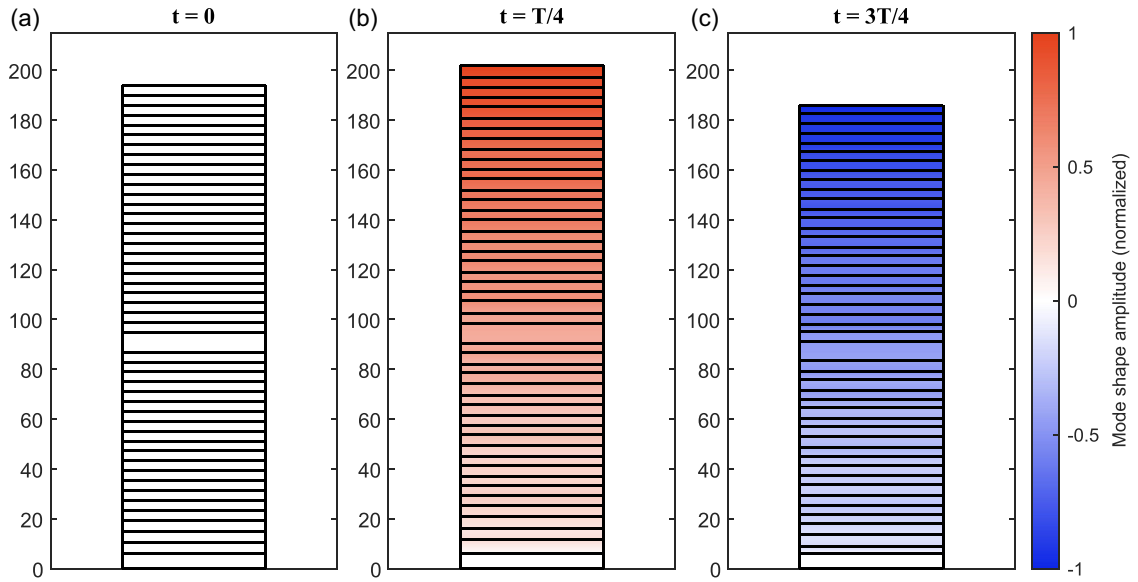

FIGURE 8 | Fundamental vertical mode shape from the state-space model using the M4.2 Malibu dataset (1.83 Hz, model order 68). Identified mode shape shown at time instants over one cycle: (a) $t = 0$ (undeformed reference), (b) $t = T/4$, and (c) $t = 3T/4$.

Since there is only one sensor per floor level, it is not possible to directly perform any floor-level dynamic identification to isolate the local slab of floor diaphragm modes. However, to further eliminate the possibility that this mode is associated with a slab mode, a separate modal analysis is conducted using a typical floor plan from a finite-element model of the building that is already constructed using ETABS software (Kohler et al. 2016; CSI 2024). A shell membrane element is used for the concrete floor slab with adjusted elastic modulus properties in the three directions to account for the metal deck and variable in-plane and out-of-plane stiffness. Columns and bracing attached to the floor slab for the floor above and below are fixed, assumed massless, and made very rigid to isolate the deformation and mass concentration to the floor slab level. Secondary beams and girders are also included, as their out-of-plane behavior significantly influences the structural elements that can stiffen the slab in the vertical direction. The floor slab modal analysis results indicate a fundamental floor slab frequency of 3 Hz, which is larger than the detected 1.86 Hz.

4 | Time–Frequency Analysis and Beating

4.1 | Methodology

To quantify beating observations, acceleration data from the vertical components are bandpass filtered for a narrow frequency band around the fundamental vertical mode identified in the previous section to understand how energy is distributed across different frequencies and time and then used in Wigner–Ville spectrogram computations. Unlike a standard spectrogram that involves dividing the signal into overlapping short time windows and computing the Fourier transform of each window, the Wigner–Ville distribution is a quadratic time–frequency distribution. It can provide more precise resolution than linear methods and is obtained by computing the Fourier transform of the time-lagged autocorrelation function of the signal (Boashash 2003; Auger and Flandrin 1995). Similar to the subspace system identification, we used only vertical signals from the earthquakes considered here (Table 1) for time–frequency analysis. Acceleration data are filtered for frequencies between 1 and 3 Hz using a Butterworth filter with three poles and zero-phase distortion to capture the energy around the fundamental mode.

4.2 | Beating Phenomenon

Some earthquakes analyzed here exhibit clear evidence of signal beating in the floor accelerations. Beating occurs when two closely spaced modal frequencies interfere leading to cyclic fluctuations in amplitude that often lead to prolonged motions from repetitive vibrational energy. This has been observed in several instrumented buildings with closely spaced horizontal and torsional periods and lightly damped systems, including in the 52-story high-rise (Boroschek and Mahin 1991; Çelebi, 2004, 2006, 2007, Çelebi et al. 2016).

Since beating leads to a periodic amplitude-modulated signal due to modal interactions, its identification can provide insight into the dynamic behavior during seismic motion. The beating effect can be modeled as the sum of two harmonic components. The beat frequency, f_b, as it is referred to in classical acoustics and wave interference theory, is approximated as the absolute difference between two frequencies ($|f_1 - f_2|$). The beating period, $T_b = 1/f_b$, is the quantity commonly reported in structural applications. The accuracy of the beating period estimation is best identified by aligning it with the amplitude envelopes of the acceleration signals. The instantaneous envelope of the acceleration time series data is obtained using the Hilbert transform (Flandrin 1999). A nonlinear regression model representing a damped sinusoidal function of the form

$$x(t) = Ae^{-2\pi(1/T_b)bt}|\sin\ (2\pi(1/T_b)t + \phi)| \tag{7}$$

where A = initial amplitude, b = damping ratio, f_b = beating frequency, t = time, and ϕ = phase angle are subsequently applied to fit the envelope of the accelerations. An initial beating period estimate is given by the high-energy node-to-node distance seen in the spectrograms.

4.3 | Spectrogram Results

Figures 9 and 10 show the spectrograms of the 2023 Malibu and 2024 Highland Park earthquakes, respectively. The spectrograms (e.g., Figure 9) capture a beating phenomenon, with energy fluctuations that appear as a spread of signal energy across slightly different frequencies. The beating effects become more pronounced with increasing height, indicating interference between two closely spaced modal frequencies in the range of 1.8–1.9 Hz. We show very similar spectrograms with the beating phenomenon for the other events in the Supporting Information (see Figures S4 and S10).

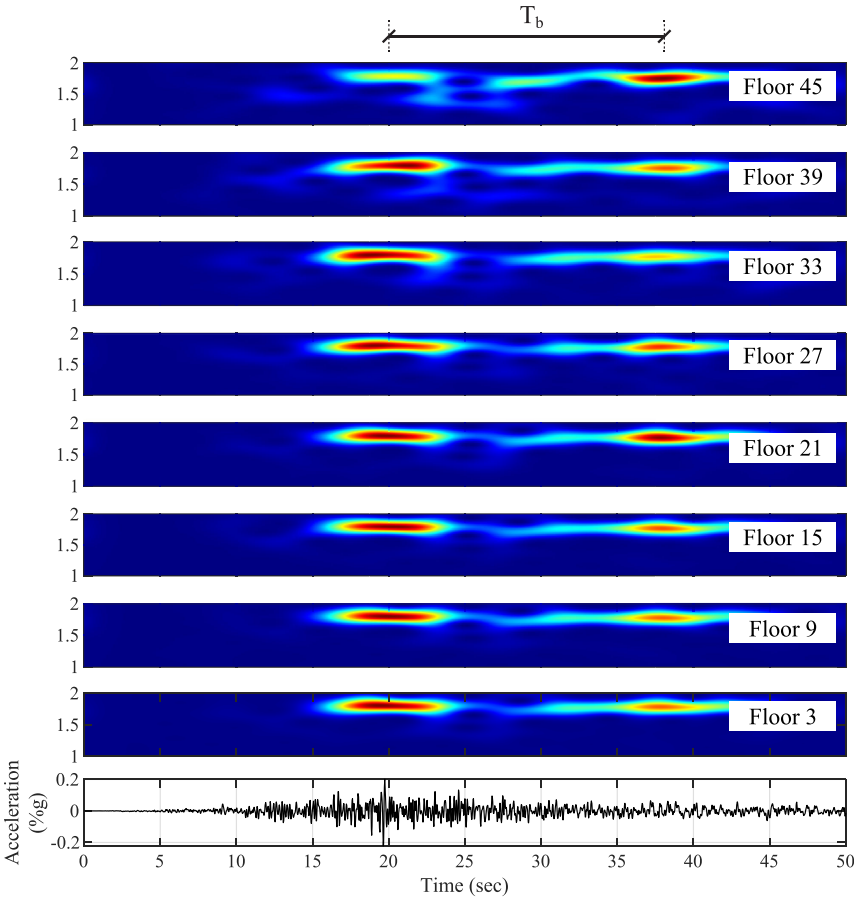

FIGURE 9 | Wigner–Ville spectrograms for the 2023 M4.2 Malibu earthquake using vertical-component CSN sensor data along the height of the 52-story high-rise. CSN = Community Seismic Network.

In this section, we also highlight the spectrogram of the 2023 Highland Park earthquake (Figure 10) despite the beating phenomenon not being as clear. It is possible that, in this particular event, there is a subtle indication of beating at the upper floor levels, above Floor 30; however, it is not as prominent. Nonetheless, these spectrogram features show a broader example of how the beating phenomenon may or may not be present.

Figure 11 shows an example of the Hilbert transform envelope and the fitted nonlinear regression model results for a single floor for the 2023 M4.2 Malibu earthquake. The beating frequencies extracted from Hilbert transform fits are consistent with the frequency difference between two closely spaced vertical modes, which span approximately from 1.8 Hz to 1.9 Hz. Peaks that reflect this frequency spacing are also observed in the vertical direction of the Fourier amplitude spectra (Figures 3 and 4). Table 3 summarizes the beating period determined from the regression model results for the various earthquakes, with no beating period determined for the 2024 M4.4 Highland Park earthquake because the beating effect is not as pronounced.

5 | TF and Temporal Changes in Modal Properties

5.1 | Methodology

TF for floor levels above ground are estimated using power spectral densities (PSDs), consistent with classical frequency response function formulations (Bendat and Piersol 2011). We adopt the PSD-based TF estimator:

$$TF(\omega) = \frac{S_{yy}(\omega)}{S_{xy}(\omega)} \tag{8}$$

where S_{yy} = auto PSD of the output signal and S_{xy} = cross PSD between input and output signal. This definition is less sensitive to input noise and provides a more robust estimate for small-amplitude recordings (Pintelon and Schoukens 2012).

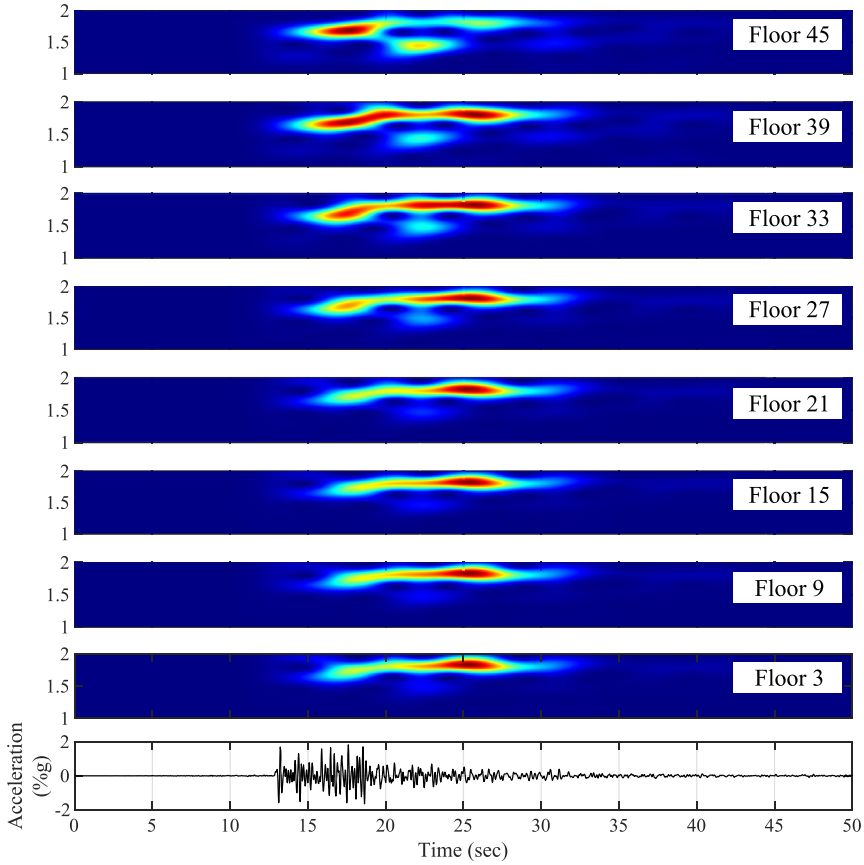

FIGURE 10 | Wigner–Ville spectrogram for the 2024 M4.4 Highland Park earthquake using vertical-component CSN sensor data along the height of the 52-story high-rise. CSN = Community Seismic Network.

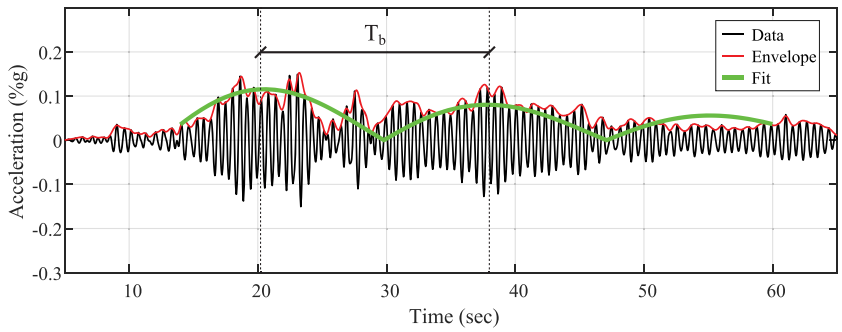

FIGURE 11 | Filtered vertical-component acceleration data with Hilbert transform envelope and nonlinear regression model fit for Floor 40 of the 52-story building for the 2023 M4.2 Malibu earthquake.

The acceleration at Floor 2 (F2) is used as the reference input signal, and PSDs are estimated by computing segmented and averaged modified periodograms using Welch's method (Welch 1967). The modal frequencies of the structure are identified by assessing the peaks in the estimated TF.

5.2 | Transfer Function Results

For each earthquake, we focused on the time segment containing most of the earthquake energy response as the best representation of building behavior during the earthquake. Figure 12 shows the TF for the vertical direction. We also computed TF in the horizontal directions (building-EW and NS) for the 2023 Malibu earthquake to compare with previously determined results to verify our method (Figure 13). The peaks in the TF observed for the building-EW and NS

TABLE 3 | Vertical mode beating period for the earthquakes using modulation envelopes from the acceleration time series.

Event	Beating period, s
2020 M4.2 Pacoima	13.51
2023 M4.2 Malibu	17.24
2024 M4.6 Malibu	11.76

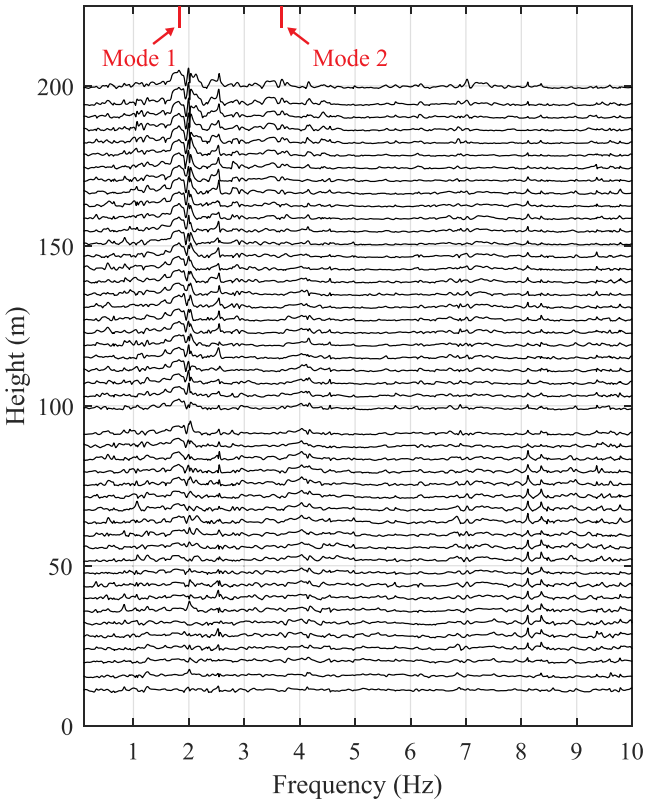

FIGURE 12 | TF computed from vertical-component acceleration signals using Floor 2 as the reference level in the 52-story high-rise from the 2023 M4.2 Malibu earthquake. Mode 1 = fundamental global vertical mode frequency. Mode 2 = second global vertical mode.

directions are the same as those reported by Kohler et al. (2016) and Ghahari et al. (2022), confirming the reliability of the method used here.

We focus particular attention on the peaks of the TF around the fundamental vertical mode identified in system identification at 1.86 Hz ± 0.03 Hz, as well as a potential second vertical mode around 3.6 Hz. Figure 12 shows spectrally distributed characteristics, with a broadband peak rather than a sharp peak, spanning a larger frequency range above the fundamental mode. The broadband spectral responses seen in the Fourier amplitude spectra around the vertical mode of 1.86 Hz (Figure 3) are also clearly present in the TF. This supports the interpretation that this is a feature of the structural response rather than a source effect or a signal-processing artifact. Tracking the peak TF amplitudes near the fundamental mode shows a top floor amplification factor of approximately 4.5 relative to F2. A weaker, but recurrent peak is occasionally observed near 3.6 Hz, as seen in Figure 12 and in other earthquakes (see Supporting Information, Figures S5 and S11), suggesting the possible presence of a second vertical mode. While this frequency lies close to the 3 Hz possible floor-slab mode obtained from the finite-element model, the TF amplitudes exhibit a height-dependent pattern that appears to correspond to a higher global vertical mode involving axial deformation rather than a localized slab vibration. This can further be supported by its intermittent appearance across events and its lower amplitude relative to the fundamental vertical mode.

TF are also computed for the 2024 Highland Park earthquake and presented in Figure 14, which shows a similar broadband peak around the fundamental mode, with a dominant peak observed at approximately 1.9 Hz. Tracking the peak TF

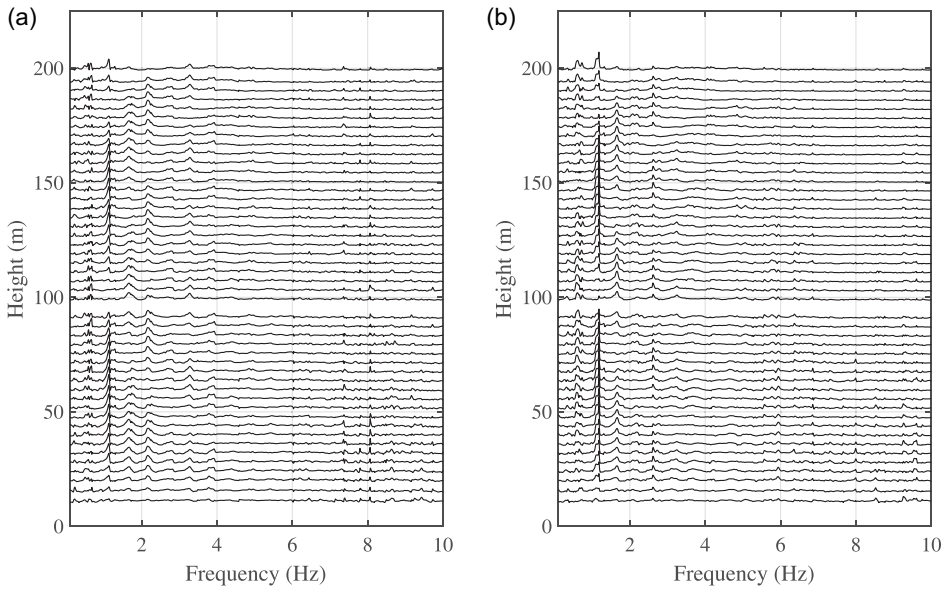

FIGURE 13 | TF obtained using acceleration signals in the (a) building-NS direction and (b) building-EW direction using Floor 2 as the reference level in the 52-story high-rise from the 2023 M4.2 Malibu earthquake.

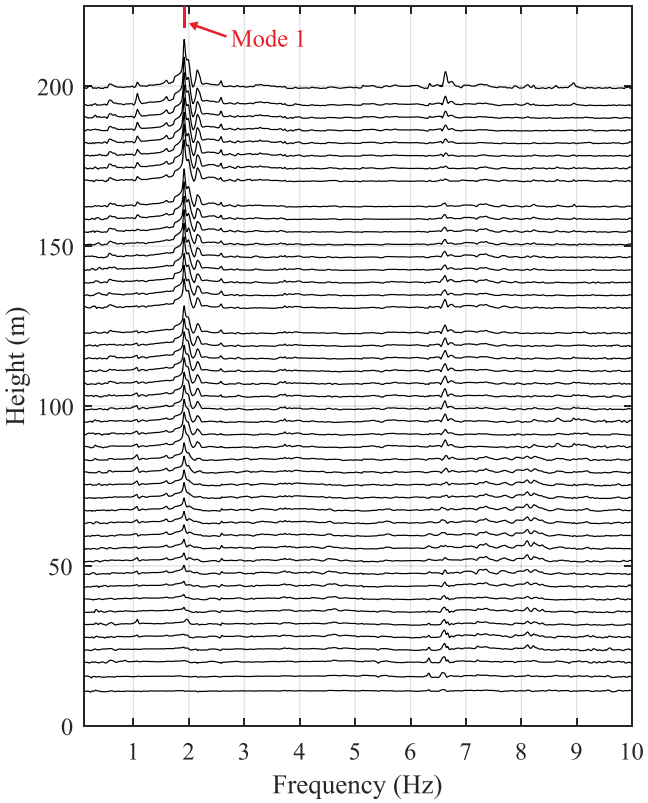

FIGURE 14 | TF computed from vertical-component acceleration signals using Floor 2 as the reference level in the 52-story high-rise from the 2024 M4.4 Highland Park earthquake. Mode 1 = fundamental global vertical mode frequency.

amplitudes near the fundamental mode reveals a top-floor amplification factor of approximately 30 relative to F2. This larger value is likely due to the closer proximity of the earthquake to the high-rise (~8 km).

We use our TF results to further study modal behavior over short-time windows (10 s) for the highest-amplitude earthquake energy portion of acceleration signals. This is to compare the temporally varying structural response during the

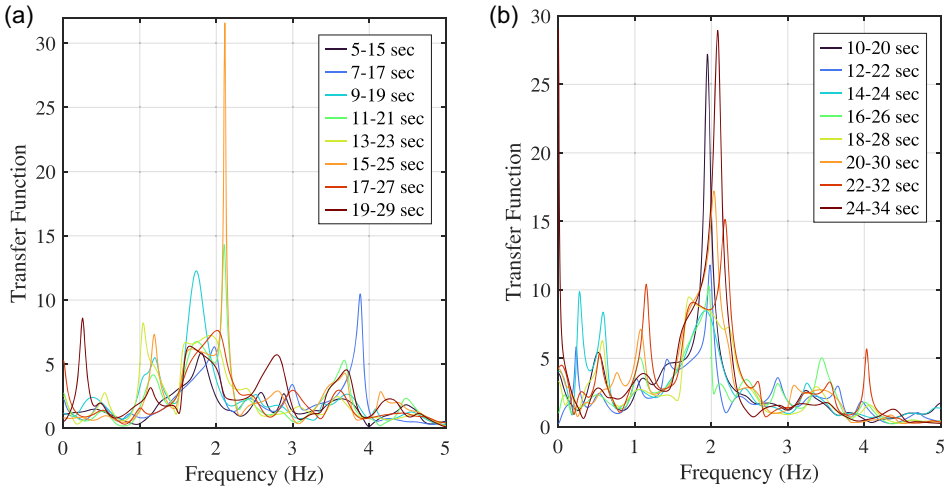

FIGURE 15 | Time-windowed TF computed from vertical-component acceleration signals recorded at Floor 45 using Floor 2 as the reference level in the 52-story high-rise. Data are from (a) the 2023 M4.2 Malibu earthquake and (b) the 2024 M4.4 Highland Park earthquake.

earthquake shaking. Figure 15 shows TF at Floor 45 associated with 10-second time-windowed shifts from records for the 2023 Malibu and the 2024 Highland Park earthquakes. Outcomes for other floor levels exhibit similar behavior.

In Figure 15a, the earlier time windows of the earthquake shaking (window start times between 5 and 20 s) show that the peaks of the TF remain concentrated around 1.8–1.9 Hz. In subsequent windows after approximately 20 s, the peak of the TF shifts upward to about 1.9–2.1 Hz. Early windows show broader, less sharply defined peaks, whereas later windows display narrower peaks. The transition from a broader to more concentrated peak coincides with the timing of peak F2 acceleration in the record. Frequencies in this range, excited simultaneously by the earthquake, are likely causing localized coupling of structural mode responses in the vertical direction, resulting in the beating phenomenon observed in the spectrograms (Figures 9 and 10).

Figure 15b shows various structural resonances within the range of 1.8–2.2 Hz. In the earlier time windows (window start times between 10 and 18 s), a peak in the TF around the fundamental vertical mode occurs between 1.88 and 2 Hz. For window start times after 20 s, the TF peak becomes dominant and steady at 2.05–2.2 Hz. Figure 15 shows clear time-varying behavior during the earthquake shaking. Since F2 is used as a reference level, the TF are relative to F2—close but not exactly the true ground level. As a result, the time-varying aspects may be influenced by the vibration intensity and its relation to the noise level at specific time windows. The detected time-varying frequencies in these windows may correspond to frequencies of the full structural system, the modified system from F2 and above, or the response in between.

We also analyze TF of ambient vibration data from before and after the earthquakes to determine whether any residual changes in dynamic behavior occurred. The 2024 M4.4 Highland Park earthquake occurred at 7:20 PM (Pacific Standard Time). We collected ambient data on the same day at 6:00 PM for pre-event and at 8:00 PM for post-event analysis. Figure 16 shows the TF from the 1-hour acceleration recordings of the ambient vibration data.

TF from both before and after the earthquakes indicate that ambient vertical vibration also excites vertical modes within the structure, consistent with the earthquake data. Small variations in peak frequency are observed across datasets, reflecting the influence of operating conditions and environmental factors. Factors such as minor nonlinearities, variations in live load, changes in temperature and humidity, wind effects, soil–structure interaction, and aging can all contribute to these shifts (Aihemaiti et al. 2024). Quantifying the contribution of each effect requires multiple datasets with varying amplitude levels and detailed numerical modeling, which are currently unavailable and beyond the scope of this work. In addition, the building's dual lateral system with outrigger constraints may introduce small, localized stiffness variations or slight mass participation shifts in the vertical direction. Numerical studies into the outrigger effect can be found in (Chen and Moehle 2024).

While our study provides new insights into the vertical dynamics of tall dual-lateral buildings, it also has limitations. The CSN sensor network does not include direct ground-level accelerometers, requiring the use of the closest instrumented floor levels, either above- or below-grade, as estimates of base excitations. Although this approximation is reasonable for

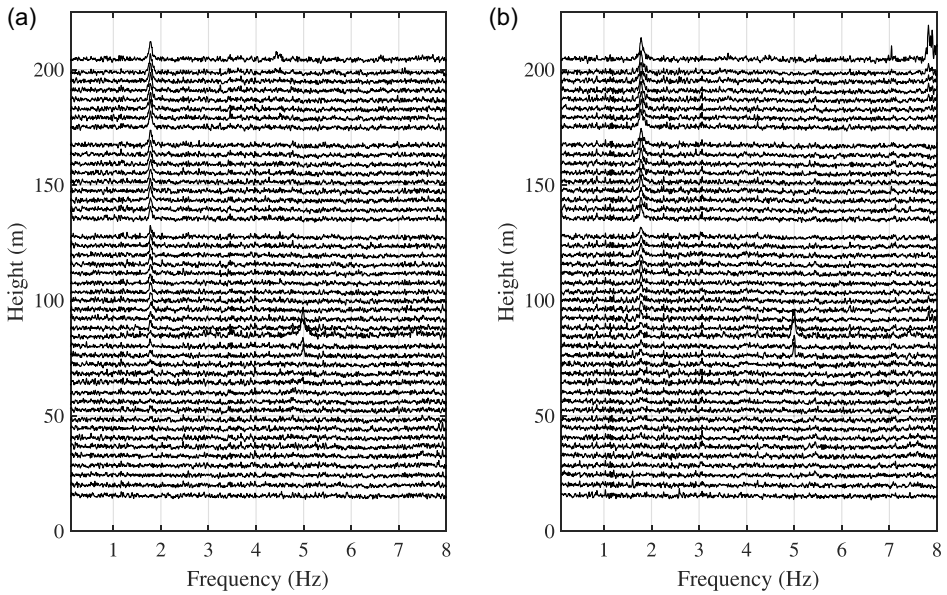

FIGURE 16 | TF from one hour of ambient vibration data recorded in the 52-story high-rise taken from (a) 6:00–7:00 PM and (b) 8:00–9:00 PM, just before and after the 2024 M4.4 Highland Park earthquake.

the low-amplitude datasets used, it may not fully capture any soil–structure interaction or large nonlinear effects that may occur during stronger shaking events.

In addition, a small number of sensors experienced data loss across different events resulting in missing signals at a floor or two. Small differences in input–output configurations can introduce minor variability in the estimated vertical dynamic parameters, which is why multiple event datasets are important to consider. The layout of sensors with only one sensor per floor near the building's central core does limit the ability to perform floor-level dynamics to eliminate any potential local mechanisms contributing to the measured vertical motion; however, the data remain valuable for capturing global system-level behavior as the identified vertical modes and beating are seen consistently across events.

6 | Conclusion

This study investigated the vertical dynamic behavior of an instrumented 52-story moment- and braced-frame high-rise in downtown Los Angeles during earthquake-induced shaking to understand the impacts of vertical seismic effects on high-rise structural analysis and design. We aim to address a critical gap in structural earthquake engineering literature, which has traditionally underestimated or overlooked the importance of vertical seismic effects in tall buildings. We collect and analyze vertical-component acceleration data from the spatially dense CSN. Using stochastic subspace state-space system identification, we systematically extracted various vertical dynamic characteristics of this dual-lateral system from spectrograms and TF of the data. Our findings indicate vertical frequencies within the range commonly produced by local earthquakes, beating phenomenon, and temporally varying frequency shifts. These observations suggest that the current seismic design oversimplifies the vertical dynamic behavior and emphasizes the need for improved vertical dynamic considerations to support more accurate vertical response predictions, which are crucial for structural integrity.

Using the vertical component of data from four small-magnitude earthquakes, we identify a fundamental vertical structural mode excited at approximately 1.86 Hz ± 0.03 Hz. This fundamental mode consists of compressional and extensional motions in the vertical direction, likely caused by overall axial extension and compression of the columns, as indicated by system model results. Due to the inherent vertical stiffness provided by the columns and core walls of tall buildings, vertical frequencies are generally assumed to fall within a higher frequency range compared to global horizontal frequencies. As a result, vertical structural modes are often overlooked under the assumption that typical earthquake ground motions will not excite these higher frequencies. However, in this study, the detected global vertical frequency of less than 2 Hz falls within a range where many local earthquakes exhibit significant energy, indicating that vertical modes can be easily excited. We expect local earthquakes to excite vertical modes across a broader portfolio of structures. In some cases, we are also able to capture a potential secondary vertical mode around 3.6 Hz excited by the earthquakes.

Subspace system identification accurately captures a stable global vertical modal frequency and suggests the presence of a potential second global mode. Using spectrograms and TF of observed waveform data, we provide quantitative and complementary insight into how vertical frequencies evolve, including the identification of a vertical beating phenomenon. Spectrogram analysis of the earthquake acceleration signals reveals the temporal frequency evolution and transient phenomena in the energy near the fundamental vertical mode, between 1.8 and 2.0 Hz, across different time windows. We document clear evidence of vertical beating in three of the four small-magnitude earthquakes characterized by beating periods ranging from 11 to 20 s. TF data are used to estimate structural response independent of seismic source effects. The TF along the height of the building consistently confirm the presence and variability of a mode in the 1.8–2.2 Hz range, indicating temporally varying dynamic behavior. Isolating the superstructure from the lower levels below ground through TF is one way to determine that the beating phenomenon is consistently present and not misinterpreted from earthquake to earthquake. During small-magnitude earthquakes, a temporary stiffening effect is observed in the vertical direction, leading to a broadband energy spread that extends to frequencies above the global fundamental vertical mode. We theorize that this can be attributed to an outrigger effect that could be occurring in this type of dual-lateral structural system. During even small-magnitude events, the outrigger moment beams may introduce stress redistribution in axial load between the inner and perimeter columns, modifying vertical mode shapes and potentially exciting a slightly higher frequency than the fundamental mode. Such behavior challenges assumptions that structures typically exhibit increased flexibility during ground shaking and warrants further investigation into why this occurs.

Increased axial loads, amplified floor accelerations, and stress redistribution in vertical elements are significant concerns in earthquake hazard design, particularly for acceleration- and fatigue-sensitive connections. Axial load changes resulting from column extension due to vertical mode excitation can impact ductility and long-term performance, particularly in high-rise structures with complex load redistribution mechanisms such as outriggers and perimeter–frame interactions. This is seen with increased floor accelerations as a function of height in a building. Increased forces resulting from constructive interference in signal beating can contribute to fatigue in structural elements or cause increased stress at critical points, such as beam-column or slab-column connections, which can be damage-inducing in certain earthquake scenarios. For lateral system elements, such as reinforced concrete columns, that typically perform well under confinement, the extension of columns can lead to a reduction in ductility and overall performance. Current empirical design factors in the building code used to estimate vertical response are overly generalized and may not adequately capture building-specific behavior highlighted by our findings. A more advanced approach is needed to incorporate vertical dynamics into three-dimensional seismic analysis, moving beyond the common practice of considering them only for vertically irregular or long-span structures.

Conflicts of Interest

The authors declare no conflicts of interest.

Data Availability Statement

The data analyzed here, including four small-magnitude earthquakes from 2020 to 2024, can be accessed through the CSN website: [http://csn.caltech.edu/]. See Supporting Information for more information on Station ID corresponding to the 52-story high-rise sensors.

References

Acosta, A. A., E. Miranda, and G. G. Deierlein 2024. "*Dynamics of Buildings in the Vertical Component.*" *Proceedings of the 18th World Conference on Earthquake Engineering*.

Acosta, A. A., E. Miranda, and G. G. Deierlein. 2023. "Response Spectrum Method for Structures Subjected to Vertical Ground Motions: Absolute Acceleration Method." *Earthquake Engineering & Structural Dynamics* 52, no. 15: 4820–4841.

AFAD. 2023. "*Disaster and Emergency Management Authority-Turkish Accelerometric Database and Analysis System (TADAS).*" https://tadas.afad.gov.tr/.

Aihemaiti, A., M. I. Todorovska, and M. D. Trifunac. 2023. "Tongde Plaza Yue Center (TPYC) Full-Scale Testbed Site: Fixed-Base Digital Twin and Its Validation Using Microtremors, Lecture Notes in Civil Engineering," In *Experimental Vibration Analysis for Civil Engineering Structures (EVACES)*, edited by M. P. Limongelli, P. F. Giordano, S. Quqa, C. Gentile and A. Cigada. 433. Springer.

Aihemaiti, A., M. I. Todorovska, M. D. Trifunac, L. Cruz, G. Lin, and J. Cui 2024. "*The Effects of Weather on the Vibrational Frequencies of an Instrumented 50-Story Skyscraper." Proceedings of the 18th World Conference on Earthquake Engineering*.

Alvin, K. F., and K. C. Park. 1994. “Second-Order Structural Identification Procedure via State-Space-Based System Identification.” *AIAA Journal* 32, no. 2: 397–406.

Auger, F., and P. Flandrin. 1995. “Improving the Readability of Time-Frequency and Time-Scale Representations by the Reassignment Method.” *IEEE Transactions on Signal Processing* 43: 1068–1089.

Bendat, J. S., and A. G. Piersol. 2011. *Random Data: Analysis and Measurement Procedures*. 4th ed. John Wiley & Sons.

Boashash, B. 2003. *Time-Frequency Signal Analysis and Processing: A Comprehensive Reference*. Elsevier.

Boroschek, R. L., and S. A. Mahin. 1991. *Investigation of the Seismic Response of a Lightly Damped Torsionally Coupled Building*. Report UCB/EERC-91/18. Earthquake Engineering Research Center, University of California.

Boroschek, R., and D. Cares. 2020. “*Dynamic Response and Design Effect of Vertical Seismic Components in Tall Buildings.” Proceedings of the 17th World Conference on Earthquake Engineering (17WCEE).*

Bozorgnia, Y., S. Mahin, and A. G. Brady. 1998. “Vertical Response of Twelve Structures Recorded during the Northridge Earthquake.” *Earthquake Spectra* 14, no. 3: 411–432.

Çelebi, M. 2004. “Responses of a 14-Story (Anchorage, Alaska) Building to Far-Distance (Mw 7.9) Denali Fault, 2002 and Near-Distance Earthquakes in 2002.” *Earthquake Spectra* 20: 693–706.

Çelebi, M. 2006. “Recorded Earthquake Responses from the Integrated Seismic Monitoring Network of the Atwood Building, Anchorage, Alaska,” *Earthquake Spectra* 22: 847–864.

Çelebi, M. 2007. “Beating Effect Identified from Seismic Responses of Instrumented Buildings.” In *Structures Congress. New Horizons and Better Practices*. 1–10. American Society of Civil Engineers.

Çelebi, M., H. S. Ulusoy, and N. Nakata. 2016. “Responses of a Tall Building in Los Angeles, California, as Inferred from Local and Distant Earthquakes.” *Earthquake Spectra* 32, no. 3: 1821–1843.

Chen, C. I., and J. P. Moehle. 2024. *A Study of the Effects of Vertical Ground Motions on Column Axial Forces in Tall Core-Wall Buildings. Proceedings of the 18th World Conference on Earthquake Engineering*.

Clayton, R., M. Kohler, R. Guy, J. Bunn, T. Heaton, and M. Chandy. 2020. “CSN/LAUSD Network: A Dense Accelerometer Network in Los Angeles Schools.” *Seismological Research Letters* 91, no. 2A: 622–630.

Clayton, R., T. Heaton, M. Chandy, et al. 2011. “Community Seismic Network.” *Annals of Geophysics* 54, no. 6: 738–747.

Clayton, R., T. Heaton, M. Kohler, M. Chandy, R. Guy, and J. Bunn. 2015. “Community Seismic Network: A Dense Array to Sense Earthquake Strong Motions.” *Seismological Research Letters* 86: 1354–1363.

Computers and Structures Inc. 2024. *ETABS: Integrated Building Design Software*, Version 22. Computers and Structures Inc.

Döhler, M., L. Mevel, and F. Hille. 2014. “Subspace-Based Damage Detection under Changes in the Ambient Excitation Statistics.” *Mechanical Systems and Signal Processing* 45, no. 1: 207–224.

Flandrin, P. 1999. *Time-Frequency/Time-Scale Analysis. Volume 10*. 1st ed. Academic Press.

Furukawa, S., E. Sato, Y. Shi, T. Becker, and M. Nakashima. 2013. “Full-Scale Shaking Table Test of a Base-Isolated Medical Facility Subjected to Vertical Motions.” *Earthquake Engineering and Structural Dynamics* 42: 1931–1949.

Geological Survey, U. S. 2020. *Updated Compilation of VS30 Data for the United States* (USGS Data Release). Geological Survey.

Ghahari, S. F., A. Baltay, M. Çelebi, G. A. Parker, J. J. McGuire, and E. Taciroglu. 2022. “Earthquake Early Warning for Estimating Floor Shaking Levels of Tall Buildings.” *Bulletin of the Seismological Society of America* 112, no. 2: 820–849.

Ghahari, S. F., F. Abazarsa, F. Nateghi, and E. Taciroglu. 2013. “Response-Only Modal Identification of Structures Using Limited Sensors.” *Structural Control and Health Monitoring* 20 no. 6: 987–1006.

Gremer, N., and C. Adam. 2023. “Vertical Floor Acceleration Spectra for Regular Steel Frame Structures.” *Structures* 55: 690–700.

Gremer, N., C. Adam, R. A. Medina, and L. Moschen. 2019. “Vertical Peak Floor Accelerations of Elastic Moment-Resisting Steel Frames.” *Bulletin of Earthquake Engineering* 17: 3233–3254.

Juang, J.-N. 1994. *Applied System Identification*. Prentice Hall.

Kohler, M. D., et al. 2021. “*The Community Seismic Network for dense, continuous monitoring of ground and structural strong motion.” SMIP21 Seminar Proceedings*. California Geological Survey (Strong Motion Instrumentation Program).

Kohler, M., A. Massari, T. Heaton, et al. 2016. “Downtown Los Angeles 52-Story High-Rise and Free-Field Response to an Oil Refinery Explosion.” *Earthquake Spectra* 32, no. 3: 1793–1820.

Kohler, M., F. Filippitzis, T. Heaton, et al. 2020. “2019 Ridgecrest Earthquake Reveals Areas of Los Angeles that Amplify Shaking of High-Rises.” *Seismological Research Letters* 91, no. 6: 3370–3380.

Kohler, M., T. Heaton, M. Cheng, and P. Singh. 2014. "*Structural Health Monitoring through Dense Instrumentation by Community Participants: The Community Seismic Network and Quake-Catcher Network.*" *Proceedings of the 10th U.S. National Conference on Earthquake Engineering*.

Ljung, L. 1999. *System Identification: Theory for the User*. 2nd ed. Prentice Hall.

Loh, K., and C. Loh. 2019. "*Building response analysis and damage detection using subspace identification methods.*" *SMIP19 Seminar Proceedings*. California Geological Survey (Strong Motion Instrumentation Program).

Marotti, E., F. Zotti, R. De Risi, A. L. Simonelli, and A. Penna. 2024. "*Vertical Acceleration in near and Far Fault Conditions.*" *Proceedings of the 18th World Conference on Earthquake Engineering*.

Moschen, L., R. A. Medina, and C. Adam. 2016. "Vertical Acceleration Demands on Column Lines of Steel Moment-Resisting Frames." *Earthquake Engineering and Structural Dynamics* 45: 2039–2060.

Nakata, N., and R. Snieder. 2014. "Monitoring a Building using Deconvolution Interferometry, II: Ambient Vibration Analysis." *Bulletin of the Seismological Society of America* 104: 204–213.

Peng, Z., and Y. Ben-Zion. 2006. "Temporal Changes of Shallow Seismic Velocity Around the Karadere-Düzce Branch of the North Anatolian Fault and Strong Ground Motion." *Pure and Applied Geophysics* 163: 567–600.

Pintelon, R., and J. Schoukens. 2012. *System Identification: A Frequency Domain Approach*. 2nd ed. John Wiley & Sons.

Prieto, G., and M. D. Kohler. 2024. "Time-Varying Damping Ratios and Velocities in a High-Rise during Earthquakes and Ambient Vibrations from Coda Wave Interferometry." *Earthquake Spectra* 40, no. 3: 2092–2115.

Prieto, G., J. Lawrence, A. Chung, and M. Kohler. 2010. "Impulse Response of Civil Structures from Ambient Noise Analysis." *Bulletin of the Seismological Society of America* 100, no. 5A: 2322–2328.

Rahmani, M., M. Ebrahimian, and M. I. Todorovska. 2015. "Time-Wave Velocity Analysis for Early Earthquake Damage Detection in Buildings: Application to a Damaged Full-Scale RC Building." *Earthquake Engineering & Structural Dynamics* 44, no. 4: 619–636.

Reinoso, E., and E. Miranda. 2005. "Estimation of Floor Acceleration Demands in High-Rise Buildings during Earthquakes." *Structural Design of Tall and Special Buildings* 14: 107–130.

Ryan, K. L., S. Soroushian, E. M. Maragakis, E. Sato, T. Sasaki, and T. Okazaki. 2016. "Seismic Simulation of an Integrated Ceiling-Partition Wall-Piping System at E-Defense. I: Three-Dimensional Structural Response and Base Isolation." *Journal of Structural Engineering* 142, no. 2: 04015130.

Skolnik, D., Y. Lei, E. Yu, and J. Wallace. 2005. "Identification, Model Updating, and Response Prediction of an Instrumented 15-Story Steel-Frame Building." *Earthquake Spectra* 22, no. 3: 781–802.

Smyth, A. W., J-S. Pei, and S. F. Masri. 2003. "System Identification of the Vincent Thomas Suspension Bridge Using Earthquake Records." *Earthquake Engineering & Structural Dynamics* 32, no. 3: 339–367.

Sun, L., J. P. Conte, M. D. Todd, et al. 2023. "Linear System Identification of the UC San Diego Geisel Library Building, Lecture Notes in Civil Engineering." In *Experimental Vibration Analysis for Civil Engineering Structures (EVACES)*, edited by M. P. Limongelli, P. F. Giordano, S. Quqa, C. Gentile and A. Cigada. 433. Springer.

Taranath, B. S. 1997. *Steel, Concrete, and Composite Design of Tall Buildings*. 2nd ed. McGraw-Hill.

Thai, H., L. DeBrunner, J. Havilicek, K. Mish, K. Ford, and A. Medda. 2007. "*Deterministic-stochastic subspace identification for bridges.*" *in Proceedings of the IEEE/SP. 14th Workshop on Statistical Signal Processing*. 749–753. IEEE.

Todorovska, M. I., and M. D. Trifunac. 2008. "Impulse Response Analysis of the Van Nuys 7-Storey Hotel during 11 Earthquakes and Earthquake Damage Detection." *Structural Control and Health Monitoring* 15: 90–116.

Van Overschee, P., and B. De Moor. 1994. "N4SID: Subspace Algorithms for the Identification of Combined Deterministic–stochastic Systems." *Automatica* 30, no. 1: 75–93.

Welch, P. D. 1967. "The use of Fast Fourier Transform for the Estimation of Power Spectra: A Method Based on Time Averaging over Short, Modified Periodograms." *IEEE Transactions on Audio and Electroacoustics* 15, no. 2: 70–73.

Supporting Information

Additional supporting information can be found online in the Supporting Information section. **Supporting Fig. S1:** (a) Acceleration time histories and (b) Fourier amplitude spectra from Floors 2 and above from the vertical component of the CSN sensors in the 52-story building in downtown Los Angeles during the 2020 M4.2 Pacoima earthquake. Acceleration amplitudes are scaled by the same constant to show comparable relative amplitudes as a function of height. **Supporting Fig. S2:** Stability plot (top) for system identification results from recorded responses to the 2020 M4.2 Pacoima earthquake and FFTs (bottom). The stability criteria are, $\Delta f < 2\%$, $\Delta\zeta < 20\%$, MAC $> 99\%$. **Supporting Fig. S3:** Comparison of N4SID model results with data for Floor 36 from the earthquakes. (a) Acceleration time series and (b) Fourier amplitude spectra. **Supporting Fig. S4:** Wigner-Ville spectrograms for the 2020 M4.2 Pacoima earthquake using vertical-component CSN sensor data along the height of the 52-story high-rise. **Supporting Fig. S5:** Transfer functions computed from vertical-component acceleration signals using Floor 2 as the reference level in the 52-story

high-rise from the 2020 M4.2 Pacoima earthquake. **Supporting Fig. S6:** Time-windowed transfer functions computed from vertical-component acceleration signals recorded at Floor 40 using Floor 2 as the reference level in the 52-story high-rise. Data are from the 2020 M4.2 Pacoima earthquake. **Supporting Fig. S7:** (a) Acceleration time histories and (b) Fourier amplitude spectra from Floors 2 and above from the vertical component of the CSN sensors in the 52-story building in downtown Los Angeles during the 2024 M4.6 Malibu earthquake. Acceleration amplitudes are scaled by the same constant to show comparable relative amplitudes as a function of height. **Supporting Fig. S8:** Stability plot (top) for system identification results from recorded responses to the 2024 M4.6 Malibu earthquake and FFTs (bottom). The stability criteria are, $\Delta f < 2\%$, $\Delta \zeta < 20\%$, MAC > 99%. **Supporting Fig. S9:** Comparison of N4SID model results with data for Floor 36 from the earthquakes. (a) Acceleration time series and (b) Fourier amplitude spectra. **Supporting Fig. S10:** Wigner-Ville spectrograms for the 2024 M4.6 Malibu earthquake using vertical-component CSN sensor data along the height of the 52-story high-rise. **Supporting Fig. S11:** Transfer functions computed from vertical-component acceleration signals using Floor 2 as the reference level in the 52-story high-rise from the 2024 M4.6 Malibu earthquake. **Supporting Fig. S12:** Time-windowed transfer functions computed from vertical-component acceleration signals recorded at Floor 40 using Floor 2 as the reference level in the 52-story high-rise. Data are from the 2024 M4.6 Malibu earthquake. **Supporting Table S1:** Station ID and associated floor level designations for the 52-story high-rise.